ISSN 1027-4510, Journal of Surface Investigation: X-ray, Synchrotron and Neutron Techniques, 2020, Vol. 14, No. 2, pp. 351–358. © Pleiades Publishing, Ltd., 2020.
Russian Text © The Author(s), 2020, published in Poverkhnost', 2020, No. 4, pp. 40–48.

On the Stability of Multilayer ZrN/SiN$_x$ and CrN/SiN$_x$ Coatings Formed by Magnetron Sputtering to High-Temperature Oxidation

I. A. Saladukhin[a], *, G. Abadias[b], **, V. V. Uglov[a, c], *, S. V. Zlotski[a], and A. A. Malashevich[a]**

[a] *Belarusian State University, Minsk, 220030 Belarus*
[b] *Prime Institute, University of Poitiers, Poitiers, 186000 France*
[c] *South Ural State University, Chelyabinsk, 454080 Russia*
**e-mail: solodukhin@bsu.by*
***e-mail: Gregory.Abadias@univ-poitiers.fr*
****e-mail: Uglov@bsu.by*

Received July 27, 2019; revised August 30, 2019; accepted August 30, 2019

Abstract—Multilayer ZrN/SiN$_x$ and CrN/SiN$_x$ coatings are formed using the method of magnetron sputtering by the consecutive sputtering of Zr (Cr) and Si_3N_4 targets upon a variation in the thickness of an individual layer from 2 to 10 nm at a substrate temperature of 300°C (ZrN/SiN$_x$ system) and 450°C (CrN/SiN$_x$ system). X-ray diffraction analysis demonstrates that multilayer ZrN/SiN$_x$ and CrN/SiN$_x$ coatings consist of nanocrystalline ZrN (CrN) layers with the preferred orientation (002) and amorphous SiN$_x$ layers. The lattice parameters of the metal nitride phase for the ZrN/SiN$_x$ and CrN/SiN$_x$ films are greater than for monolytic ZrN and CrN layers, respectively, and, in the case of ZrN/SiN$_x$ films, the lattice parameter increases upon a reduction of the ratio of ZrN to SiN$_x$ elementary-layer thicknesses, which can be associated with the growth of compressive stress. As wavelength dispersive X-ray spectrometry of the film composition and scanning electron microscopy of the surface show, the multilayer ZrN/SiN$_x$ and CrN/SiN$_x$ coatings are more resistant to high-temperature oxidation (in the temperature range of 400–950°C) in comparison with the ZrN and CrN coatings. This resistance increases upon a decrease in the ratio of the thickness of the ZrN individual layer to that of the SiN$_x$ individual layer as well as upon an increase in the quantity of layers in the film. However, these factors are not so deciding in the case of CrN/SiNx system. In general, CrN/SiN$_x$ coatings are more stable than ZrN/SiN$_x$ coatings under the conditions of high-temperature oxidation.

Keywords: multilayer coatings, transition-metal nitride, annealing in air, stability to oxidation
DOI: 10.1134/S1027451020020512

INTRODUCTION

Films based on transition metal (TM) nitrides, such as TiN, CrN, ZrN, and others, have became widespread as solid protective coatings. The resistance of these coatings to an aggressive environment, in particular, high-temperature oxidation, a chemically aggressive environment (as exemplified by solutions of salts or acids), as well as ion radiation is one of their important characteristics. Under these conditions, mononitride films often lose their protective function. One example is that they are intensely oxidized at 550°C and higher [1, 2].

An increase in the resistance of coatings to oxidation is provided by both metallic components (Al, Zr, Ta, and others) [1, 3–6] and nonmetallic elements, such as C or Si [2, 7–11].

Another variant, which increases the resistance to high-temperature oxidation (along with an improvement in the mechanical characteristics), is the development of multilayer film structures [5, 12–15]. Unique mechanical properties can be obtained using this approach, which differ from those of single-layer coatings. One example is that the authors from [16] showed that formation and motion of dislocations in CrN/AlN multilayer coatings is not a decisive factor of plastic deformation. The observed plastic deformation is mainly caused by the rotation of nanocrystallites and grain-boundary sliding in the case of larger crystallites. Such an inelastic effect eliminates or weakens deformation and crack formation, which makes the CrN/AlN multilayer structure promising as a protective coating including for ductile steel substrates. It was mentioned in [17, 18] that CrVN/TiN and AlCrN/TiVN multilayer coatings are characterized by a higher wear resistance than CrVN and TiN or AlCrN and TiVN coatings. In the case of an AlCrN/TiVN film, AlCrN layers effectively inhibit oxygen diffusion into the film upon high-temperature annealing, which prevents the oxidation of vanadium [18].

The studies show that the degree of mutual diffusion of the components of individual single layers

Table 1. Deposition parameters and composition of the ZrN, CrN, and Si_3N_4 mononitride coatings

Film	T_d, °C	Zr Power, W	Cr Power, W	Si_3N_4 Power, W	Working pressure, Pa	Nitrogen pressure, Pa	Film thickness, nm	Zr, at %	Cr, at %	Si, at %	N, at %
ZrN	300	300	–	–	0.20	4.6×10^{-3}	249	46.6	–	–	53.4
CrN	450	–	200	–	0.20	6.3×10^{-2}	259	–	54.6	–	45.4
Si_3N_4	300	–	–	176	0.22	2.4×10^{-2}	287	–	–	43.3	56.7

through the interface between layers is an important factor, which affects the physical and mechanical characteristics of multilayer coatings. A large difference in the characteristics of TM_1/TM_2 multilayer systems from M_1/M_2 systems was mentioned in [19, 20]. Even a lower interpenetration of components is intrinsic for multilayer coatings, where the layers of transition-metal nitrides alternate with layers of SiN_x, which is caused by the mutual insolubility of these two phases [14, 21, 22]. A high thermal stability of the multilayer structure is possible due to this fact. In addition, the presence of a large number of interfaces between layers inhibits the formation of a columnar structure of the coating [21], which in turn prevents the formation of the continuous pores. The mentioned factors allow one to consider these multilayer coatings as promising materials operating under high-temperature corrosion conditions. However, the oxidative resistance of such has been insufficiently investigated to date.

In this work, the stability of ZrN/SiN_x and CrN/SiN_x coatings possessing various values of the thickness of individual layers upon annealing in air is compared.

EXPERIMENTAL

Films of ZrN, CrN, and Si_3N_4 mononitrides, as well as ZrN/SiN_x and CrN/SiN_x multilayer films were formed through reactive magnetron sputtering in a high-vacuum chamber (initial pressure is $<10^{-5}$ Pa) equipped with three confocal targets and a cryogenic pump [23]. The coatings were deposited onto Si substrates with a thin surface layer of SiO_2 10 nm in thickness (in order to avoid diffusion of the coating components into the substrate). To carry out elemental analysis of the films in the initial state, ZrN, CrN and Si_3N_4 mononitrides were also deposited onto carbon substrates. During deposition, a constant bias voltage of –60 V was applied to the substrate; the substrate rotated at a speed of 15 rpm in order to provide uniform deposition rate across the substrate surface.

Targets of Zr (99.2% purity), Cr (99.95% purity), and Si_3N_4 (99.99%) that are 7.62 cm in diameter at a distance of 18 cm from the substrate holder were sputtered by $Ar + N_2$ plasma in the constant power mode. The Zr and Cr targets were employed in the configuration of unbalanced magnetron sputtering using a direct-current power supply, while in the case of the Si_3N_4 target a high-frequency power source in the balanced magnetron-sputtering mode was used. The working pressure in the chamber corresponded to 0.20 Pa upon the deposition of ZrN and CrN layers and 0.22 Pa in the case of SiN_x layers (Table 1); in this case, measurements were performed using a Baratron capacitance sensor. On the basis of previous experiments [24, 25], the Ar-to-N_2 gas-flow ratio to the chamber was optimized in order to obtain a nitrogen content in the coating close to stoichiometric. The partial N_2 pressure was controlled during deposition using an MKS Microvision mass spectrometer.

The growth of ZrN monotride films and ZrN/SiN_x multilayer films was carried out at a substrate temperature of 300°C, while the substrate temperature corresponded to 450°C in the case of CrN mononitride films and CrN/SiN_x multilayer films. Films of Si_3N_4 were obtained at both temperatures.

In the case of multilayer films, periodic growth of the layers was controlled by computer-controlled pneumatic shutters at a distance of 2 cm from each target. The deposition started from the ZrN (CrN) layer. A more detailed description of the procedure and features of formation of the multilayer coatings is given in [22]. Table 1 shows the deposition conditions of the mononitride coatings and the same conditions were used during the formation of individual layers of ZrN/SiN_x and CrN/SiN_x structures except for the time of deposition, which was specified for the necessary layer-thickness values. The total film thickness of all types was nearly 300 nm. The thickness ratio of individual layers in the ZrN/SiN_x multilayer films was 2 nm/5 nm, 5 nm/5 nm, 5 nm/10 nm, 10 nm/10 nm, and 10 nm/5 nm. In the case of CrN/SiN_x films, this value corresponded to 2 nm/5 nm, 5 nm/5 nm, 5 nm/10 nm, and 10 nm/5 nm.

The elemental composition of the deposited films, as well as the films exposed to annealing in air was determined by X-ray microanalysis (XMA). XMA was carried out using an Oxford Instruments spectrometer coupled with a JEOL 7001F-TTLS scanning electron microscope (SEM). The XMA spectra were recorded at a voltage of 10 kV and a probe current of 10 nA. In the case of the Si_3N_4 films, which possess a lower den-

sity, a voltage of 5 kV and a probe current of 5 nA were used. Reduced voltage and probe-current values were chosen in order to eliminate the contribution of the substrate (the signal of the substrate element at the background level). Calculations were carried out using INCA Energy+ software. Using the same microscope, the film surface topography after air annealing was analyzed.

In order to determine the structural-phase state of the films, X-ray analysis was used. X-ray analysis was carried out using a D8 Bruker diffractometer in the Bragg–Brentano configuration with CuK_α radiation (wavelength is 0.15418 nm, Lynx Eye detector).

The specimens were annealed in air sequentially at various temperatures in the range of 400–950°C. The oxidation process was analyzed in situ. The specimens were placed on an object table equipped with a resistive heater and transferred to the Bruker D8 diffractometer. The table represented a specimen holder made from AlN and a hemispherical graphite dome exposed to air blowing. The time of recording during isothermal annealing at each temperature corresponded to 40–60 min.

RESULTS AND DISCUSSION

Structural–Phase Composition of the Initial ZrN/SiN$_x$ and CrN/SiN$_x$ Multilayer Films

The elemental composition of individual layers in the multilayer systems corresponds to the composition of ZrN, CrN, and Si_3N_4 mononitride films in Table 1. During the XMA study of the coatings deposited onto Si substrates, oxygen was detected (within 1.5–2.0 at. %), which can be caused by the presence of a thin oxide layer both on the film surface and 10-nm SiO_2 layer on the substrate surface.

As shown by transmission electron microscopy in [22], layers without discontinuities possessing plane-parallel and clearly distinguishable boundaries are formed as a result of the successive deposition of individual layers of ZrN and SiN$_x$. In this case, even thin layers possessing a thickness of 1 nm were rather well distinguishable, which clearly demonstrates the absence of interpenetration of the elements between the ZrN and SiN$_x$ layers.

Figures 1 and 2 show fragments of the X-ray diffraction patterns in the case of ZrN/SiN$_x$ and CrN/SiN$_x$ multilayer films. There are two most intense (111) and (200) peaks of the ZrN phase and only one (200) peak of the cubic phase of CrN in the specified angle range. It should be noted that no other lines were recorded in the entire reflection-angle range ($2\theta = 20°–65°$) except for ZrN mononitride, in which a weak reflection was recorded corresponding to the 2θ angle 56.38° ((220) line). Therefore, it is possible to state the evolution of the structural state of the ZrN phase only in terms of the (111) and (200) lines and the (200) line in the case of the CrN phase.

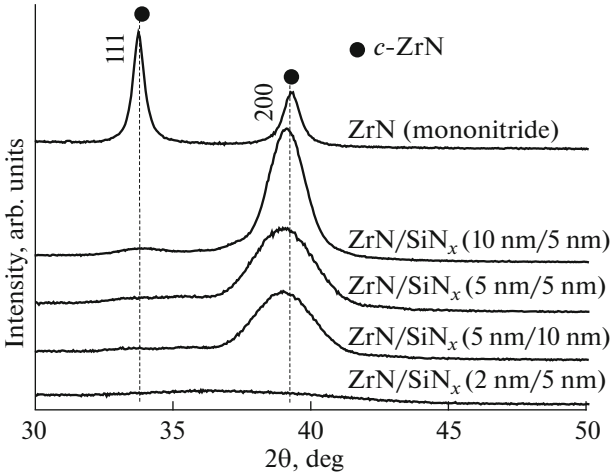

Fig. 1. X-ray diffraction patterns of ZrN mononitride coating and ZrN/SiN$_x$ multilayer coatings at various ZrN-SiN$_x$ layer thickness ratios in the initial state.

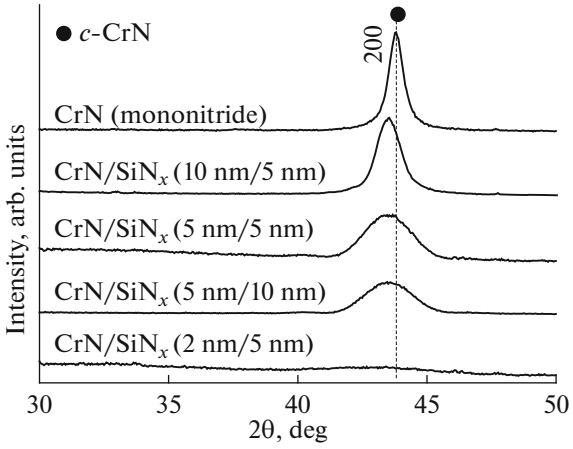

Fig. 2. X-ray diffraction patterns of CrN mononitride coating and CrN/SiN$_x$ multilayer coatings at various CrN-SiN$_x$ layer thickness ratios in the initial state.

As follows from Fig. 1, there is a transition from (111) preferred orientation of zirconium-nitride crystallites to the (200) orientation with the addition of an intermediate layer of SiN$_x$ between the ZrN layers. At a ZrN-SiN$_x$ layer thickness ratio of 5 : 5 nm, there is an increase in the full width at half maximum of the diffraction peak, as well as a decrease in its intensity. At a thickness ratio of 2 : 5 nm, the film becomes almost X-ray amorphous.

The observed evolution of the (111) and (200) peaks of the ZrN phase in the multilayere films can be related to the following structural changes. In the case of ZrN/SiN$_x$ films, the addition of a SiN$_x$ layer results in the inhibition of columnar growth of the grains of the ZrN phase with (111) preferred orientation and a significant increase in the lattice parameter as compared to the ZrN mononitride film (Table 2). Growth

Table 2. Lattice parameter of the transition-metal nitride phase (ZrN or CrN) depending on the type of coating

Type of coating	Lattice parameter a, Å
Mononitrides	
ZrN	4.590
CrN	4.133
ZrN/SiN_x multilayer coatings	
ZrN/SiN_x (10 nm/5 nm)	4.611
ZrN/SiN_x (10 nm/10 nm)	4.613
ZrN/SiN_x (5 nm/5 nm)	4.628
ZrN/SiN_x (5 nm/10 nm)	4.629
ZrN/SiN_x (2 nm/5 nm)	–
CrN/SiN_x multilayer coatings	
CrN/SiN_x (10 nm/5 nm)	4.159
CrN/SiN_x (5 nm/5 nm)	4.162
CrN/SiN_x (5 nm/10 nm)	4.159
CrN/SiN_x (2 nm/5 nm)	–

of the lattice parameter (usually) is accompanied by the growth of compressive stresses. In this case, the largest increase in the lattice parameter of the ZrN phase in the ZrN/SiN_x multilayer coatings occurs with a decrease in the ZrN-layer thickness to 5 nm and less. As mentioned above, there is an increase in the full width at half maximum of the diffraction-peak maximum from 1.6° in the case of the ZrN-SiN_x layer thickness ratio corresponding to 10 : 5 nm to 3.1° in the case of 5 : 5 nm. The latter fact may indicate a significant decrease in the crystallite size in the ZrN layers with a decrease in their thickness.

As pointed above, only the diffraction maximum corresponding to the line (200) is recorded for the CrN mononitride coating. One peak is also recorded for the CrN/SiN_x multilayer coatings (Fig. 2). In this case, the lattice parameter of the CrN phase of the multilayer coatings is also significantly higher than that of the CrN monitride film (Table 2). As in the case of the ZrN/SiN_x films, there is diffraction-peak broadening with a decrease in the CrN-SiN_x layer thickness ratio, which can indicate a decrease in the crystallite size. However, the angular position of the diffraction peak does not change significantly. The latter implies that the compressive-stress values remain at the same level at the considered individual layer thickness ratios.

Thus, there are the following main principles of structural changes of the ZrN and CrN phases in the ZrN/SiN_x and CrN/SiN_x multilayer films:

(i) the presence of (200) preferred orientation;

(ii) exceedance of the lattice parameter as compared to that of ZrN and CrN mononitride coatings, which indicates the presence of compressive stresses;

(iii) a decrease in the crystallite size with a decrease in the ZrN (or CrN) layer thickness at a constant thickness of the SiN_x layer;

(iv) ZrN/SiN_x (or CrN/SiN_x) multilayer films become X-ray amorphous (as in the case of the Si_3N_4 mononitride film) with a decrease in the ZrN (or CrN) layer thickness to 2 nm.

Resistance of ZrN/SiN_x and CrN/SiN_x Multilayer Films to Oxidation upon Annealing in Air

The results of the X-ray analysis of ZrN and CrN mononitride films in comparison with ZrN/SiN_x and CrN/SiN_x multilayer films during annealing in air in the temperature range of 400–950°C are given in Figs. 3 and 4. As follows from these figures, oxidation of the ZrN films starts at 550°C and the diffraction maximum corresponding to the zirconium-nitride phase at 700°C is not recorded, while the peaks of m-ZrO_2 and t-ZrO_2 are observed (Fig. 3a). At the same time, the CrN films starts to oxidize at 700°C and the peak corresponding to the CrN phase disappears at 860°C (Fig. 4a). In this case, peaks corresponding to the t-Cr_2O_3 oxide arise.

Oxidation of the ZrN/SiN_x multilayer films starts at 860–950°C (Figs. 3b, 3c) and the peak of the t-ZrO_2 oxide phase starts to be resolved only at 950°C. In the case of the coating with a ZrN-SiN_x layer thickness ratio of 5 : 5 nm, the peak of the ZrN phase disappears only at 950°C (Fig. 3b). With a decrease in the ZrN-SiN_x layer thickness ratio, the resistance of the film to oxidation increases; i.e., the peak corresponding to the zirconium-nitride phase in the case of ZrN/SiN_x coatings (5 nm/10 nm) is recorded up to a temperature of 950°C (Fig. 3c). It should be noted that the ZrN/SiN_x film (2 nm/5 nm) is X-ray amorphous in the initial state and remains the same after annealing. In this case, the oxide phases are not detected. The latter can be related to the fact that this film at the same total thickness (~300 nm) consists of a larger number of individual layers. This can provide an increase in its stability upon oxidation due to an increase in the density of boundaries between layers, which represents a factor preventing oxygen diffusion into the film. The state of the ZrN layer in this film close to amorphous, which is related to ultrasmall grain size, also inhibits oxygen diffusion along the grain boundaries.

Analysis of the resistance to oxidation of CrN/SiN_x multilayer coatings upon annealing in air in the temperature range of 400–950°C (Fig. 4) indicates their significantly higher stability as compared to ZrN/SiN_x multilayer coatings. At all the CrN-SiN_x layer thickness ratios of 5 : 5 nm, 5 : 10 nm, and 2 : 5 nm, the oxide phase is not detected using X-ray analysis and the peak of the CrN phase almost retains its intensity up to a temperature of 950°C (Figs. 4b, 4c). The structure of the CrN/SiN_x multilayer film with an individual layer

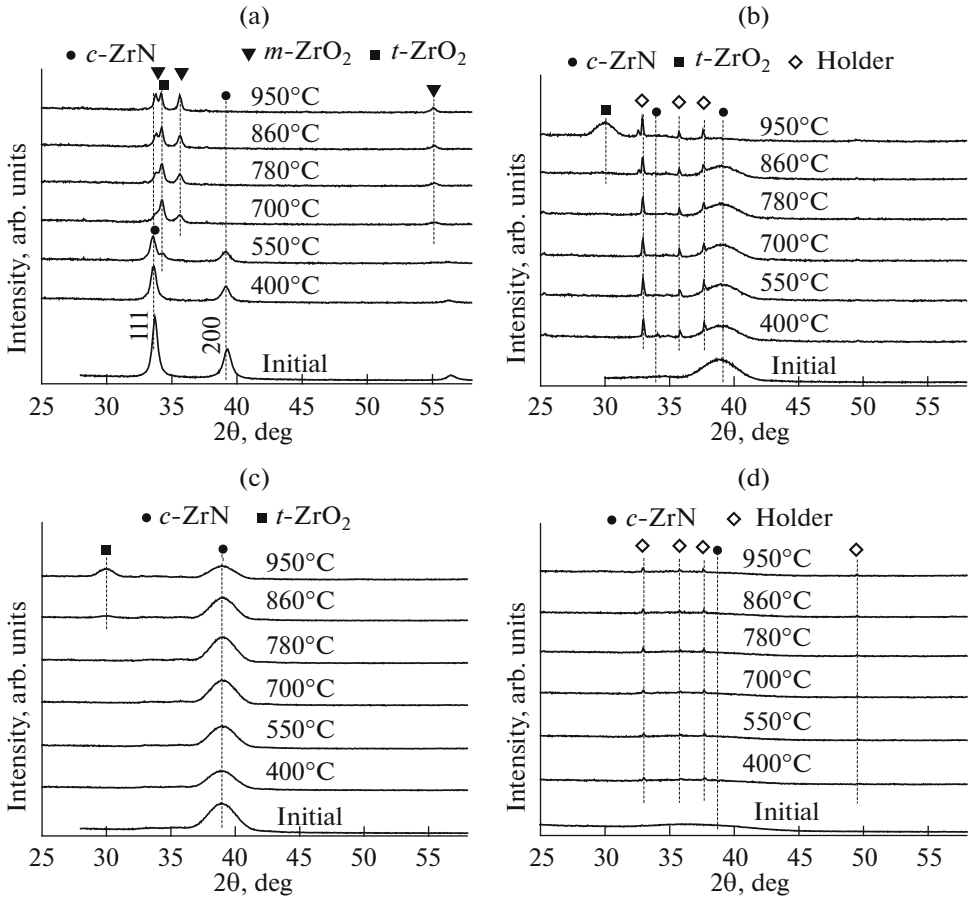

Fig. 3. X-ray diffraction patterns of the (a) ZrN mononitride coating and ZrN/SiN$_x$ multilayer coatings at various ZrN-SiN$_x$ layer thickness ratios of (b) 5 nm/5 nm, (c) 5 nm/10 nm, and (d) 2 nm/5 nm annealed in air.

thickness ratio of 2 : 5 nm remains X-ray amorphous at all temperatures of annealing (Fig. 4d) as in the case of the ZrN/SiN$_x$ system (Fig. 3d).

Elemental analysis of the ZrN and CrN mononitride films and ZrN/SiN$_x$ and CrN/SiN$_x$ multilayer films after annealing in air is given in Table 3. As follows from the table, in the case of the ZrN/SiN$_x$ system, the film with the ZrN-SiN$_x$ film thickness ratio of 2 : 5 nm possesses the highest resistance to high-temperature oxidation. The film thickness-mean nitrogen content after annealing corresponds to 33.1 at. %, which is significantly higher as compared to other ZrN/SiN$_x$ multilayer coatings. It should be noted that the integral content of elements corresponding to the bulk coating is given in Table 3. For this reason, these data allow one to compare the resistance of multilayer films to oxidation in two systems, ZrN/SiN$_x$ and CrN/SiN$_x$, with identical individual-layer thickness ratios.

A significantly lower oxygen content in the CrN/SiN$_x$ multilayer films exposed to annealing in air should be noted (Table 3). In contrast to the CrN mononitride film, which was oxidized completely, the oxygen content in the CrN/SiN$_x$ multilayer films after annealing is 14–19 at %. It should be noted that, in contrast to the ZrN/SiN$_x$ system, the oxidation rate does not change significantly upon varying the thickness-ratio values in the case of CrN/SiN$_x$ films with CrN-SiN$_x$ individual layer thickness ratios of 10 : 5 nm, 5 : 5 nm, 5 : 10 nm, and 2 : 5 nm. Nevertheless, the lowest oxygen content in the CrN/SiN$_x$ film with a CrN-SiN$_x$ individual layer thickness ratio of 10 : 5 nm is presumably caused by the predominant role of chromium oxide as a passivating film under high-temperature annealing conditions. This represents a clear difference between the CrN/SiN$_x$ system and the ZrN/SiN$_x$ system, in which the predominance of the SiN$_x$ layer thickness to that of ZrN is a factor, which increases the resistance of the coating to high-temperature oxidation.

Figures 5–7 show the surface topography of the ZrN, CrN, and Si$_3$N$_4$ mononitride films (Fig. 5) and ZrN/SiN$_x$ (Fig. 6) and CrN/SiN$_x$ multilayer coatings (Fig. 7) annealed in the temperature range of 400–950°C. A high degree of damage upon annealing of the ZrN and CrN mononitride coatings should be noted (Figs. 5a, 5b). In the former case, a high density of cor-

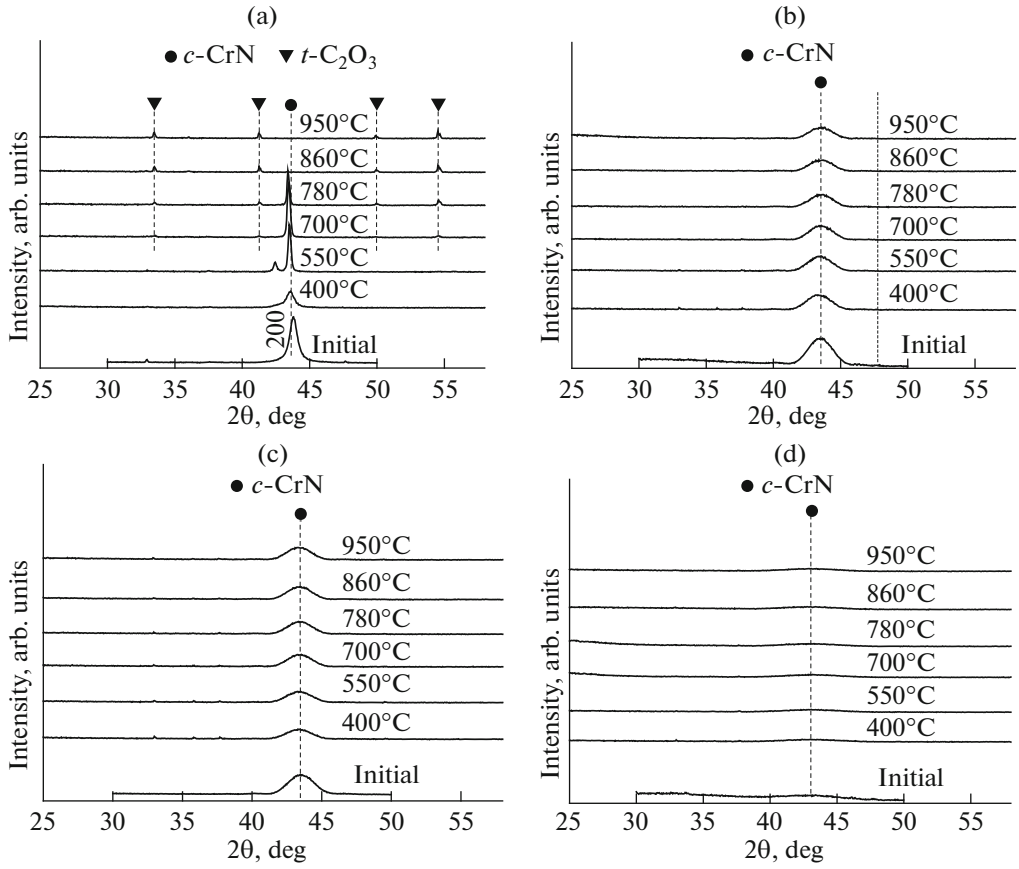

Fig. 4. X-ray diffraction patterns of the (a) CrN mononitride coating and CrN/SiN_x multilayer coatings at various CrN-SiN_x layer thickness ratios of (b) 5 nm/5 nm, (c) 5 nm/10 nm, and (d) 2 nm/5 nm annealed in air.

Table 3. Results of elemental analysis of the ZrN, CrN, and SiN_x mononitride coatings, as well as ZrN/SiN_x and CrN/SiN_x multilayer coatings after annealing in air in the temperature range of 400–950°C

Film	Zr, at %	Cr, at %	Si, at %	N, at %	O, at %
Mononitrides					
ZrN	27.8	–	–	–	72.2
CrN	–	37.3	–	–	62.7
Si_3N_4	–	–	32.0	40.0	28.0
ZrN/SiN_x multilayer coatings					
ZrN/SiN_x (10 nm/5 nm)	17.4	–	14.0	1.0	67.6
ZrN/SiN_x (5 nm/5 nm)	12.0	–	20.1	3.6	64.3
ZrN/SiN_x (5 nm/10 nm)	10.4	–	25.7	17.8	46.1
ZrN/SiN_x (2 nm /5 nm)	9.1	–	30.3	33.1	27.5
CrN/SiN_x multilayer coatings					
CrN/SiN_x (10 nm/5 nm)	–	32.6	13.8	39.3	14.3
CrN/SiN_x (5 nm/5 nm)	–	20.2	21.2	41.0	17.6
CrN/SiN_x (5 nm/10 nm)	–	13.1	26.0	43.7	17.2
CrN/SiN_x (2 nm/5 nm)	–	12.2	28.5	40.2	19.1

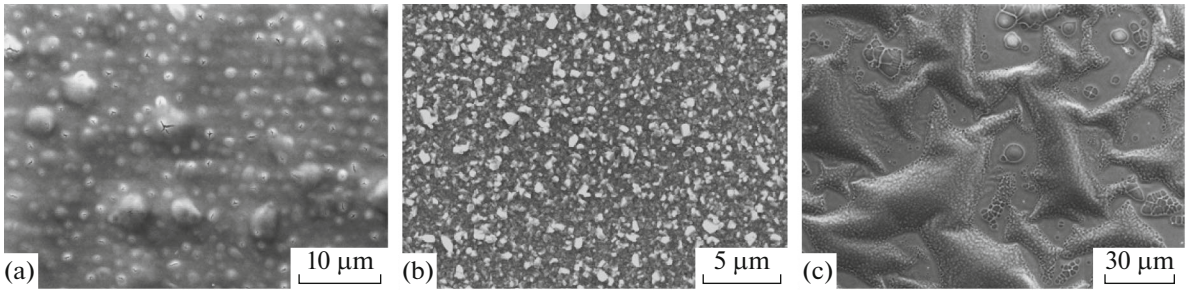

Fig. 5. Surface topography of the (a) ZrN, (b) CrN, and (c) Si_3N_4 mononitride coatings annealed in air.

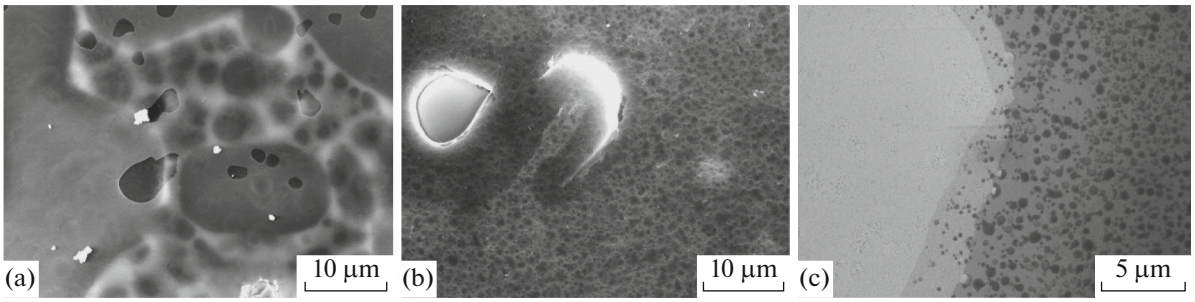

Fig. 6. Surface topography of the ZrN/SiN$_x$ multilayer coatings at various ZrN-SiN$_x$ layer thickness ratios of (a) 5 nm/5 nm, (b) 5 nm/10 nm, and (c) 2 nm/5 nm annealed in air.

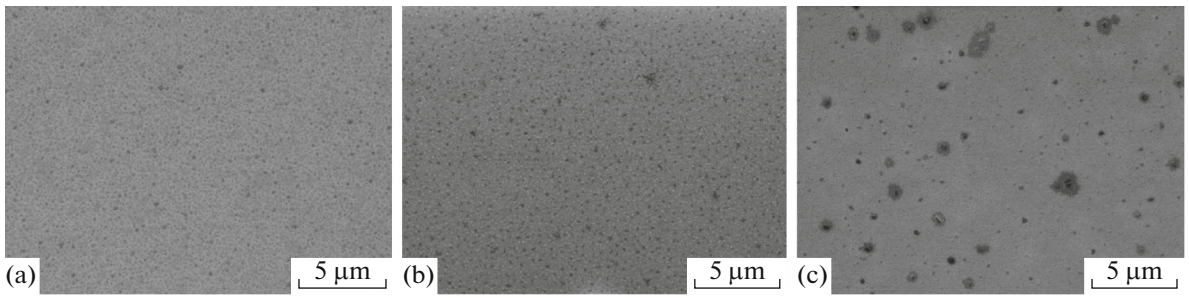

Fig. 7. Surface topography of the CrN/SiN$_x$ multilayer coatings at various CrN-SiN$_x$ layer thickness ratios of (a) 5 nm/5 nm, (b) 5 nm/10 nm, and (c) 2 nm/5 nm annealed in air.

rosion centers, which result in swelling of the coating, is observed (Fig. 5a). In the latter case, there is intense cracking and flaking of the coating (Fig. 5b). Intense delayering as a result of annealing is also observed in the Si_3N_4 films (Fig. 5c).

In the case of the ZrN/SiN$_x$ coatings, the degree of damage of the surface in the case of high-temperature corrosion significantly decreases with a decrease in the ZrN-SiN$_x$ layer thickness ratio (Figs. 6a–6c).

In the case of the CrN/SiN$_x$ films, isolated sites of high-temperature corrosion arise at all thickness-ratio values (Figs. 7a–7c). However, these sites usually do not transform into complexes, which results in the absence of delayering regions of the coating resulting in distortion of its integrity.

Thus, the X-ray analysis, XMA, and SEM analysis of ZrN/SiN$_x$ and CrN/SiN$_x$ multilayer coatings allow a conclusion regarding their higher resistance to high-temperature oxidation as compared to ZrN and CrN mononitride coatings. In this case, the CrN/SiN$_x$ system has the greatest effect.

CONCLUSIONS

ZrN/SiN$_x$ and CrN/SiN$_x$ multilayer coatings formed through magnetron sputtering represent alternating nanocrystalline layers of the ZrN (CrN) phase possessing (002) preferred orientation and amorphous layers of SiN$_x$. The lattice parameter of the metal nitride phase in the multilayer structures exceeds the lattice parameter corresponding to the ZrN and CrN

mononitride films, which indicates the presence of compressive stresses. During the formation of ZrN/SiN_x and CrN/SiN_x multilayer structures, a decrease in the ZrN (CrN)-SiN_x layer thickness ratio results in a decrease in the crystallite size of the metal nitride phase.

Analysis of the ZrN/SiN_x and CrN/SiN_x multilayer films allows a conclusion regarding their higher resistance to high-temperature oxidation as compared to the ZrN, CrN, and Si_3N_4 mononitride films.

Resistance of the ZrN/SiN_x films to oxidation increases with a decrease in the ZrN individual-layer thickness to that of SiN_x, as well as an increase in the number of layers in the film.

The CrN/SiN_x films possess a significantly higher resistance to high-temperature oxidation as compared to the ZrN/SiN_x films. In this case, the CrN-SiN_x individual layer ratio is not a decisive factor.

FUNDING

The work was supported by the Belarusian Republic Foundation for Basic Research (project no. F18MC-027).

REFERENCES

1. G. Abadias, L. E. Koutsokeras, A. Siozios, and P. Patsalas, Thin Solid Films **538,** 56 (2013). https://doi.org/10.1016/j.tsf.2012.10.119
2. H. C. Barshilia, B. Deepthi, A. S. Arun Prabhu, and K. S. Rajam, Surf. Coat. Technol. **201,** 329 (2006). https://doi.org/10.1016/j.surfcoat.2005.11.124
3. S. G. Harris, E. D. Doyle, A. C. Vlasveld, et al., Wear **254,** 723 (2003). https://doi.org/10.1016/S0043-1648(03)00258-8
4. L. Chen, L. He, Y. Xu, et al., Surf. Coat. Technol. **244,** 87 (2014). https://doi.org/10.1016/j.surfcoat.2014.01.063
5. C. M. Koller, R. Hollerweger, C. Sabitzer, et al., Surf. Coat. Technol. **259,** 599 (2014). https://doi.org/10.1016/j.surfcoat.2014.10.024
6. M. Pfeiler, G. A. Fontalvo, J. Wagner, et al., Tribol. Lett. **30,** 91 (2008). https://doi.org/10.1007/s11249-008-9313-6
7. M. Stueber, U. Albers, H. Leiste, et al., Surf. Coat. Technol. **200,** 6162 (2006). https://doi.org/10.1016/j.surfcoat.2005.11.012
8. R. Wei, C. Rincon, and E. Langa, J. Vac. Sci. Technol., A **28** (5), 1126 (2010). https://doi.org/10.1116/1.3463709
9. H. C. Barshilia, B. Deepthi, and K. S. Rajam, Surf. Coat. Technol. **201,** 9468 (2007). https://doi.org/10.1016/j.surfcoat.2007.04.002
10. Y. H. Cheng, T. Browne, B. Heckerman, and E. I. Meletis, Surf. Coat. Technol. **204,** 2123 (2010). https://doi.org/10.1016/j.surfcoat.2009.11.034
11. Y.-I. Chen, Y.-X. Gao, and L.-C. Chang, Surf. Coat. Technol. **332,** 72 (2017). https://doi.org/10.1016/j.surfcoat.2017.09.087
12. K. Yalamanchili, I. C. Schramm, E. Jiménez-Piqué, et al., Acta Mater. **89,** 22 (2015). https://doi.org/10.1016/j.actamat.2015.01.066
13. T. Weirather, K. Chladil, B. Sartory, et al., Surf. Coat. Technol. **257,** 48 (2014). https://doi.org/10.1016/j.surfcoat.2014.06.018
14. X. Bai, W. Zheng, T. An, and Q. Jiang, J. Phys.: Condens. Matter **17,** 6405 (2005). https://doi.org/10.1088/0953-8984/17/41/011
15. I. A. Saladukhin, G. Abadias, V. V. Uglov, et al., Surf. Coat. Technol. **332,** 428 (2017). https://doi.org/10.1016/j.surfcoat.2017.08.076
16. K. Bobzin, T. Brögelmann, N. C. Kruppe, et al., Surf. Coat. Technol. **332,** 253 (2017). https://doi.org/10.1016/j.surfcoat.2017.06.092
17. E. Contreras, Y. Galindez, and M. A. Rodas, Surf. Coat. Technol. **332,** 214 (2017). https://doi.org/10.1016/j.surfcoat.2017.07.086
18. Y.-Y. Chang, S.-Y. Weng, C.-H. Chen, and F.-X. Fu, Surf. Coat. Technol. **332,** 494 (2017). https://doi.org/10.1016/j.surfcoat.2017.06.080
19. D. Peruško, M. J. Webb, V. Milinović, et al., Nucl. Instrum. Methods Phys. Res., Sect. B **266,** 1749 (2008). https://doi.org/10.1016/j.nimb.2008.02.034
20. I. Kim, L. Jiao, F. Khatkhatay, et al., J. Nucl. Mater. **441,** 47 (2013). https://doi.org/10.1016/j.jnucmat.2013.05.035
21. T. P. Soares, C. Aguzzoli, G. V. Soares, et al., Surf. Coat. Technol. **237,** 170 (2013). https://doi.org/10.1016/j.surfcoat.2013.09.061
22. G. Abadias, V. V. Uglov, I. A. Saladukhin, et al., Surf. Coat. Technol. **308,** 158 (2016). https://doi.org/10.1016/j.surfcoat.2016.06.099
23. J. J. Colin, Y. Diot, P. Guerin, et al., Rev. Sci. Instrum. **87,** 023902 (2016). https://doi.org/10.1063/1.4940933
24. G. Abadias, L. E. Koutsokeras, S. N. Dub, et al., J. Vac. Sci. Technol., A **28,** 541 (2010). https://doi.org/10.1116/1.3426296
25. L. Simonot, D. Babonneau, S. Camelio, et al., Thin Solid Films **518,** 2637 (2010). https://doi.org/10.1016/j.tsf.2009.08.005

Translated by A. Muravev